Geohazard Mechanics 2 (2024) 244–257

Contents lists available at ScienceDirect

Geohazard Mechanics

journal homepage: www.keaipublishing.com/en/journals/geohazard-mechanics

# Indirect evaluation of the influence of rock boulders in blasting to the geohazard: Unearthing geologic insights fused with tree seed based LSTM algorithm

Blessing Olamide Taiwo [a,b], Shahab Hosseini [c], Yewuhalashet Fissha [d,e,**], Kursat Kilic [d], Omosebi Akinwale Olusola [a], N. Sri Chandrahas [f], Enming Li [g,*], Adams Abiodun Akinlabi [a], Naseer Muhammad Khan [h,i]

[a] Department of Mining Engineering, Federal University of Technology, Akure, 340001, Nigeria
[b] HNF Global Resources Limited, Akoko Edo, Nigeria
[c] Faculty of Engineering, Tarbiat Modares University, Tehran, 14117, Iran
[d] Department of Geosciences, Geotechnology and Materials Engineering for Resources, Graduate School of International Resource Sciences, Akita University, Akita, 0108502, Japan
[e] Department of Mining Engineering, Aksum University, Aksum, 7080, Ethiopia
[f] Mine Planning Division, GMMCO Technology Services (GTS), Hyderabad, 500008, India
[g] School of Mine and Energy, Polytechnic University of Madrid, Madrid, 28003, Spain
[h] Department of Sustainable Advanced Geomechanical Engineering, Military College of Engineering, National University of Sciences and Technology, Risalpur, 23200, Pakistan
[i] MEU Research Unit, Middle East University, Amman, 11831, Jordan

ARTICLE INFO

*Keywords:*
Oversize boulder
Blasting
Image analysis
Downstream operation
Artificial intelligence

ABSTRACT

Effective control of blasting outcomes depends on a thorough understanding of rock geology and the integration of geological characteristics with blast design parameters. This study underscores the importance of adapting blast design parameters to geological conditions to optimize the utilization of explosive energy for rock fragmentation. To achieve this, data on fifty geo-blast design parameters were collected and used to train machine learning algorithms. The objective was to develop predictive models for estimating the blast oversize percentage, incorporating seven controlled components and one uncontrollable index. The study employed a combination of hybrid long-short-term memory (LSTM), support vector regression, and random forest algorithms. Among these, the LSTM model enhanced with the tree seed algorithm (LSTM-TSA) demonstrated the highest prediction accuracy when handling large datasets. The LSTM-TSA soft computing model was specifically leveraged to optimize various blast parameters such as burden, spacing, stemming length, drill hole length, charge length, powder factor, and joint set number. The estimated percentage oversize values for these parameters were determined as 0.7 m, 0.9 m, 0.65 m, 1.4 m, 0.7 m, 1.03 kg/m$^3$, 35 %, and 2, respectively. Application of the LSTM-TSA model resulted in a significant 28.1 % increase in the crusher's production rate, showcasing its effectiveness in improving blasting operations.

## 1. Introduction

Rock geology play a pivotal role in dictating the efficacy of all blasting operations, determining both economic viability and risk mitigation. A meticulous selection of design parameters, informed by a comprehensive understanding of the site's geological characteristics, is paramount in ensuring optimal outcomes that adhere to global standards for safety and cost-effectiveness [1]. Likewise, the understanding helps in reducing and matching explosive energy to suit the requirements like desired rock fragmentation sizes [2].

* Corresponding author.
** Corresponding author. Department of Geosciences, Geotechnology and Materials Engineering for Resources, Graduate School of International Resource Sciences, Akita University, Akita, 0108502, Japan.
*E-mail addresses:* yowagaye@gmail.com (Y. Fissha), enming.li@alumnos.upm.es (E. Li).

https://doi.org/10.1016/j.ghm.2024.06.001
Received 6 May 2024; Received in revised form 11 June 2024; Accepted 26 June 2024
Available online 27 June 2024
2949-7418/© 2024 The Author(s). Publishing services by Elsevier B.V. on behalf of KeAi Communications Co. Ltd. This is an open access article under the CC BY-NC-ND license (http://creativecommons.org/licenses/by-nc-nd/4.0/).

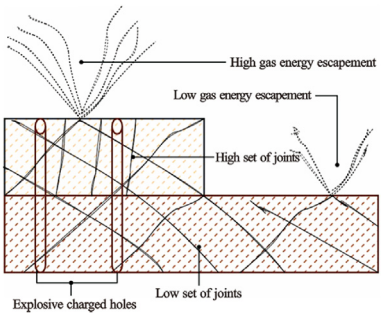


**Fig. 1.** Schematic representation of joints influence on explosive energy utilization.

For the last couple of centuries, rock excavation with explosives has been the most used method in mining, road construction, tunnelling, and others have utilized billions of tons of explosives [3]. As a result, productivity and efficiency increased significantly, contributing significantly to economic growth and modern living standards. A blasted rock muck pile and the fragment sizes contained within it are critical for the mining industry because they affect downstream processes ranging from loading to crushing. Singh and Narendrula [4] assert that oversized material poses a significant challenge to the loading, transportation, and crushing equipment used in an operation. The presence of large boulders (oversized material) in blasted muck not only reduces output but also raises the cost of loading and downstream operation systems. Several attempts have been made to improve blasting results using empirical models and machine learning techniques, most of which have been hampered by the soft computing state, making adoption and usage difficult for the mining industry. Attempts have also been made for decades to improve blasting efficiency in order to reduce costs and increase production. The majority of these efforts involve trial-and-error techniques aimed at changing a single output and do not include geological discontinuities like joints and bedding plane [5].

According to Calnan [6], explosive energy is composed of five primary components: rock fragmentation, heave, ground vibration, air blast, and heat. Fragmentation and heave are regarded as beneficial components, whereas the remainder is regarded as waste and is responsible for the blast's environmental impact. According to Calnan [6], these two beneficial components account for less than 30 % of the total explosive energy proportion of the blast. The remaining 70 % is wasted, escaping through geological discontinuities such as rock joints [7] as shown in Fig. 1. Despite the limited energy fraction available, blasting results in oversize, undersize, and optimum fragment size distribution due to human factors, poor design, and the blasting approach. There are two ways to optimize the downstream operation: using explosive energy optimally to produce less oversize run-of-mine material and utilizing an improved comminution machine to enhance both crushing and grinding rates [8].

Oversized rocks from blasting operations adversely impact loading and subsequent mining activities by causing equipment blockages, increasing loading cycle times, and necessitating secondary breakage. These inefficiencies lead to increased operational costs and reduced production efficiency [9]. Additionally, blast generated oversized rocks pose significant safety risks, including potential equipment damage and an increased likelihood of hazardous manual handling by workers, thereby elevating the risk of accidents and injuries. Addressing these issues is crucial for optimizing mining operations and ensuring worker safety.

To avoid environmental effects and financial uncertainties, an approach that matches explosive utilization is better than opting for the comminution procedure. Explosive utilization can be maximized when it is understood and integrated with the rock geology, including joints [10].

Furthermore, inadequate rock blasting designs, characterized by factors such as excessive powder usage or insufficient burden distance, pose significant risks, including geological disasters like landslides and ground subsidence [11]. These flaws are identifiable through blast result assessments due to their association with nonuniform fragmentation and oversize material production [12,13]. The development and application of accurate simulation models are imperative for predicting blast outcomes and mitigating associated hazards. Through simulating blasting outputs, engineers can optimize parameters, thereby reducing disaster probabilities, minimizing environmental impact, protecting infrastructure, and enhancing safety. This underscores the pivotal role of simulation in fostering responsible blasting practices.

The optimization of loading energy consumption on the basis of blast fragmentation size distribution minimizes the total cost that drilling and blasting design parameters can generate, as well as the cost required to mill one ton of ore [14,15]. In general, the energy consumption rate during loading is the sum of three major components: swinging energy, digging energy, and crowd energy, whereas the downstream energy consumption consists primarily of fracturing energy during impacting and transportation costs between processing circuits [8,16].

Various empirical models and soft computing models can predict the size distribution of the blasted muck pile based on blast design controllable and uncontrollable parameters, such as rock strength, stemming, burden, drill hole diameter, bench height, and powder factor. Researchers have found that these models accurately predict the mean fragment size and the 80 % passing size, but they fail to factor in the oversize and undersize particle sizes that determine energy consumption during loading and downstream operations. The prediction of blasting boulder distribution is tough due to the fact that the rock fracturing process is complicated which might involve the rock fracture creation, propagation, and penetration. Gong et al. [17] have made valuable efforts to investigate such fracturing behavior by developing an effective numerical method. In addition, the influence of transverse isotropy [18] and size effect [19] on the deformability and strength of the rock is difficult to understand under dynamic loading. Regarding this, artificial intelligence models are considered to be employed because they can provide reasonable trends for potential geotechnical hazards [20–23] and fragmentation resulting from blast design parameter adjustments [9]. The purpose of this study will be to expand the findings of a safe and productive mining system and improve fundamental understanding of how blast fragmentation size distribution affects downstream operations based on artificial intelligence techniques. Long-term memory networks (LSTMs), for instance, are descendants of recurrent neural networks (RNNs) and can be used to solve complex problems such as the generation of blast-oversize fractions. RNNs can learn sequential patterns from data containing temporal or sequential information. The LSTM model will be created to predict the percentage of oversized material in blast fragments in terms of size distribution. Rather than deep feed-forward neural networks, RNN-based methods for learning temporal patterns have recently been applied to time-series data analysis models [24]. An approach based on LSTM networks that can avoid vanishing gradient difficulties [25] and reflect long-term dependency has gained popularity among RNN methodologies [26]. In this study, therefore, deep long-term memory networks optimized with gray wolf optimizer (GWO), particle swarm optimization (PSO), and tree seed algorithm (TSA) were considered and compared with random forest (RF) and support vector regressions with attention to sigmoid kernel (SVR-S), Gaussian-RBF Kernel (SVR-RBF), linear Kernel (SVR-L), and polynomial Kernel (SVR-P) functions.

## 2. Review of machine learning application to fragmentation

The method used to move fragmented materials from the pile to the haul truck bucket is known as the loading operation. Awuah-Offei's review work [27] on energy efficiency in mining mentioned this operation as requiring high energy consumption and having a significant impact on the fleet operation. The mining industry's downstream operation begins with the primary crusher, the machine with the largest inlet size for

**Table 1**
Literature review of machine learning application to rock fragmentation prediction.

| Reference | Year | Technique | Number of datasets | $R^2$ |
|---|---|---|---|---|
| [39] | 2009 | FIS | 415 | 0.96 |
| [40] | 2010 | ANN | 250 | 0.98 |
| [41] | 2011 | ANN | 220 | 0.97 |
| [42] | 2013 | ANN | 103 | 0.85 |
| [43] | 2013 | ANFIS | 30 | 0.83 |
| [44] | 2015 | FIS, LMR | 185 | FIS = 0.922<br>LMR = 0.738 |
| [45] | 2016 | ANN-ABC | 34 | 0.78 |
| [46] | 2016 | RES, NLMR | 52 | RES = 0.866<br>NLMR = 0.777 |
| [47] | 2018 | ANN-FA | 200 | 0.94 |
| [48] | 2020 | CSO | 75 | 0.985 |
| [49] | 2022 | ANN, SVR | 102 | ANN = 0.87, SVR = 0.81 |
| [50] | 2022 | XGBoost, RF, KNN | 152 | XGBoost = 0.9125, RF = 0.67, KNN = 0.87 |
| [51] | 2022 | GEP | 1032 | 0.981 |
| [52] | 2022 | LMR, NLMR, RES | | LMR = 0.759, NLMR = 0.801, RES = 0.931 |

Fuzzy inference system is short for FIS, artificial neural network for ANN, adaptive neuro-fuzzy inference system for ANFIS, linear multiple regression for LMR, artificial bee colony for ABC, rock engineering system for RES, non-linear multiple regression for NLMR, firefly algorithm for FA, cat search optimization for CSO, support vector regression for SVR, eXtreme gradient boosting for XGBoost, random forest for RF, K-Nearest Neighbors for KNN, and gene expression programming for GEP.

receiving run-off mines for further size reduction. The blast fragment size and the efficiency of the primary crusher's inlet matching determine the blasting and downstream operation productivity. According to Kinyua et al.'s review work [8] on fragmentation's influence on downstream operations, the particle size of the run-of-mine ore and the degree of internal micro fracturing in the fragments induced by blasting have been identified as the two key aspects of rock fragmentation that influence downstream mineral processing operations. Singh et al. [28] found that blast results impact the efficiency of comminution equipment, energy consumption, and mineral recovery. According to Awuah-Offei et al. [29], an increase in blasting energy leads to energy savings in mining operations as a whole and facilitates energy reduction in combustion circuits. Due to the fact that the energy efficiency of comminution processes is very low based on the energy required to generate new fracture surface area relative to the mechanical (strain) energy input, optimizing blast fragment size will contribute to reducing energy consumption and optimizing downstream operations. During crowding and digging, the rate at which an operator executes a particular bucket-load trajectory is directly proportional to the amount of power consumed. However, faster loading speeds reduce cycle times, which boosts productivity and should improve energy efficiency. Manyele [30] mentioned that shift availability for excavators, loading location, excavator model, and truck-shovel combinations have a significant impact on productivity during the loading process in an open-pit mine. There are various approaches for analysing rock fragmentation, each with its own set of restrictions, resulting in varied variational prediction errors. The rock fragmentation model, according to Moomivand et al. [31], is a critical tool in blasting operations for design and parameter modelling. Several attempts have been made to build various blast particle size distribution prediction models, including the use of artificial intelligence algorithms and soft computing methodologies [32–34]. Furthermore, the development of fragmentation models offers novel solutions to blasting difficulties, such as improved mine-to-mill fragmentation products [8,35,36]. Bhatawdekar et al. [37] observed the availability of many developed models for predicting blast fragmentation size distribution. Based on the nature of the forecast result and the model creation technique, these models can be classified as empirical, mechanistic, or soft computing. In the last four decades, several academics have attempted to investigate the effect of blast parameters and rock qualities on fragmentation. However, there has been a great deal of debate, which is mostly due to the small number of field experiments, the lack of fundamental understanding of how rock deformation nature influences fracture, and the large diversity in the results. Taiwo [35] investigates the impact of charge loading proportion on fragmentation outcome. The study noted that the assessment of blast results is a significant approach for the improvement of mining operations. Bhatawdekar et al. [38] employed 105 data sets to create a hybrid model for blast fragmentation prediction that combined an artificial neural network (ANN) with particle swarm optimization (PSO), known as PSO-ANN. The findings reveal that artificial neural network-based algorithms can forecast fragmentation. Amoako et al. [34] used ANN and support vector machines to estimate blast mean size, with coefficients of determination of 0.87 and 0.81, respectively. Table 1

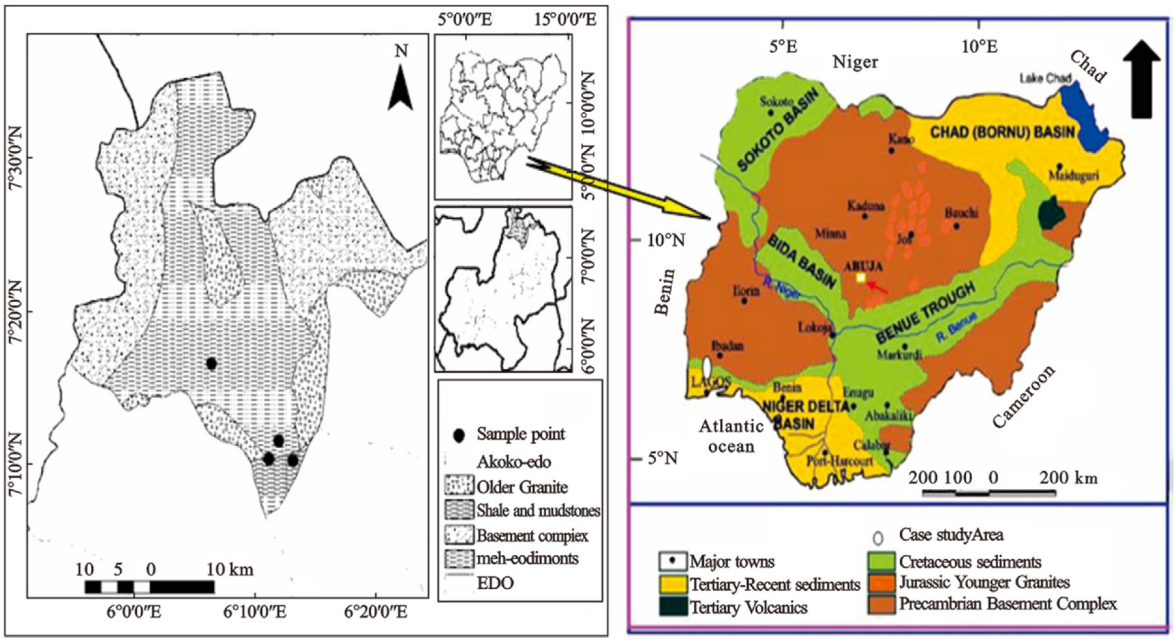


**Fig. 2.** Geological map of Akoko Edo, showing case study area.

**Table 2**
Field data statistics.

| Parameter | Input | | | | | | | | No of joints sets | Output |
|---|---|---|---|---|---|---|---|---|---|---|
| | Burden (m) | Spacing (m) | Stemming (m) | Hole depth (m) | Burden to spacing ratio | Charge length (m) | Brittleness index | Powder factor (kg/m$^3$) | | Oversize boulder (cm) |
| Sign | *B* | *S* | *T* | *H* | *B/S* | *CL* | *BI* | *PF* | *Jn* | *OB* |
| Mean | 0.83 | 1.06 | 0.66 | 1.30 | 0.79 | 0.64 | 6.69 | 0.77 | 2 | 50.83 |
| Median | 0.82 | 1.07 | 0.66 | 1.30 | 0.79 | 0.64 | 5.46 | 0.74 | 3 | 51.76 |
| Mode | 0.80 | 1.20 | 0.66 | 1.30 | 0.67 | 0.64 | 7.57 | 0.70 | 5 | 53.90 |
| Standard Deviation | 0.11 | 0.12 | 0.10 | 0.10 | 0.10 | 0.07 | 3.51 | 0.20 | | 10.67 |
| Kurtosis | 2.76 | 0.37 | 4.24 | 27.48 | 2.57 | 4.65 | 2.06 | 14.27 | | 0.38 |
| Skewness | 0.97 | −0.33 | −1.10 | −4.51 | 1.05 | −0.52 | 1.68 | 2.77 | | −0.38 |
| Range | 0.60 | 0.60 | 0.61 | 0.75 | 0.52 | 0.42 | 14.25 | 1.36 | | 46.21 |
| Minimum | 0.60 | 0.70 | 0.29 | 0.70 | 0.65 | 0.40 | 3.22 | 0.44 | | 23.31 |
| Maximum | 1.20 | 1.30 | 0.90 | 1.45 | 1.17 | 0.82 | 17.47 | 1.80 | | 69.52 |

shows prior implementations of the machine learning approach to estimating rock particle size distributions.

Existing methods for predicting rock blast oversize may suffer from limited ability to capture complex temporal patterns and dependencies in the data [53]. Hybrid Long Short-Term Memory (LSTM) models offer advantages by combining the strengths of LSTM networks with other techniques, such as statistical methods or traditional machine learning algorithms. This hybrid approach can improve predictive accuracy by leveraging LSTM's ability to handle sequential data while mitigating the limitations of standalone LSTM models, resulting in more robust and accurate predictions. This current study cross validates the proposed model using testing data and training data from different geological conditions as represented by the rock brittleness parameter.

## 3. Field study

### 3.1. Data description

Methods for predicting blast fragmentation size induced by blasting activity have been developed through research. A dataset gathered from the Akoko Edo dolomite quarry was used for blast oversize prediction, and machine learning prediction models were constructed based on the primary blasting parameters. The information was gathered from a dolomite quarry in Akoko Edo local government area, Edo state, Nigeria (Fig. 2). A blast hole diameter of 40 mm is bored vertically in the mine using staggered and square drill-hole patterns to depths ranging from 0.7 to 1.45 m. Non-electric (NONEL) detonators, packed emulsion gel as the bottom charge load, and 0.8 g/cc ANFO as the column charge load are used in explosive charging. Each explosion's controllable blast design parameters were documented. For the case study rock brittleness index estimation, the rock strength characteristics, including uniaxial compressive strength and Brazilian tensile strength, were determined in accordance with the *International Society of Rock Mechanics Commission* [54]. Using Eq. (1), the brittleness index was derived.

$$\mathrm{BI} = \frac{UCS}{D_t} \tag{1}$$

where *UCS* is the uniaxial compressive strength, MPa; $D_t$ is the tensile strength, MPa.

Table 2 displays the dataset statistics used to develop and evaluate machine learning models. Eight metrics, including the burden to spacing ratio, stemming length, hole depth, charge length, brittle index, and powder factor, and joint set numbers are presented for each blast case in the data. This study's overall methodology starts with the gathering of field data, model construction, and analysis of prediction accuracy using five performance indices. The sequential method employed in this study is shown in Fig. 3. The range and other statistical analyses of the model parameters are shown in Table 2 and Fig. 4, respectively.

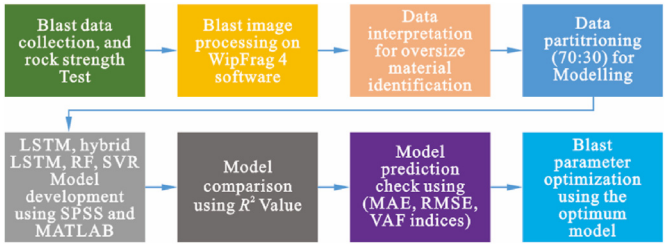


**Fig. 3.** A flowchart of the Research work.

### 3.2. Image analysis for blast result assessment

Nanda and Pal [55] assert that assessing blast fragmentation on a large scale is a highly challenging task, and extensive research has been conducted utilizing several approaches and tools to evaluate fragmentation. Common ways for quantifying fragmentation include the over-sized boulder count method, sifting or screening, and the shovel loading rate method. Contemporary approaches include the visual analysis method, the photogrammetric method, and the image analysis method. WipFrag is an image analysis method used to measure the size distributions of materials, such as blasted or crushed rock [55]. The image analysis software is promoted as an advanced framework for gravimetry based on photographs. It is mainly designed for photos with great contrast in gray tones, although it can also identify coloured prints [56]. The two-dimensional net is quantified, and a three-dimensional distribution is reconstructed utilizing principles of geometric probability [57]. In this study, 50 photographs were captured to analyse the fragmentation of the dolomite quarry. The photos were taken after the blast muck pile and after 10 loading stockpile spreads. The methodology used in this study to measure blast fragmentation is illustrated in Fig. 5. The edge detection variable (EDV) is a useful tool for analysing the boundaries of fragments. The calibration technique was employed to manually increase the edges of the rock particles, hence improving accuracy. The WipFrag particle distribution cumulative curves were analysed using fifty blast photographs to calculate the proportion of oversize material based on the outlet area size of the main crusher in the case study mine [12].

## 4. Blast oversize model development

### 4.1. Long-term memory networks (LSTMs) for the predictions of blast oversize

Long short-term memory networks (LSTMs), a subclass of RNNs, are gaining popularity [58,59]. LSTMs minimize the vanishing gradient/exploding gradient issue of regular RNNs by effectively capturing long-term dependencies utilizing memory cells and gates [24]. The

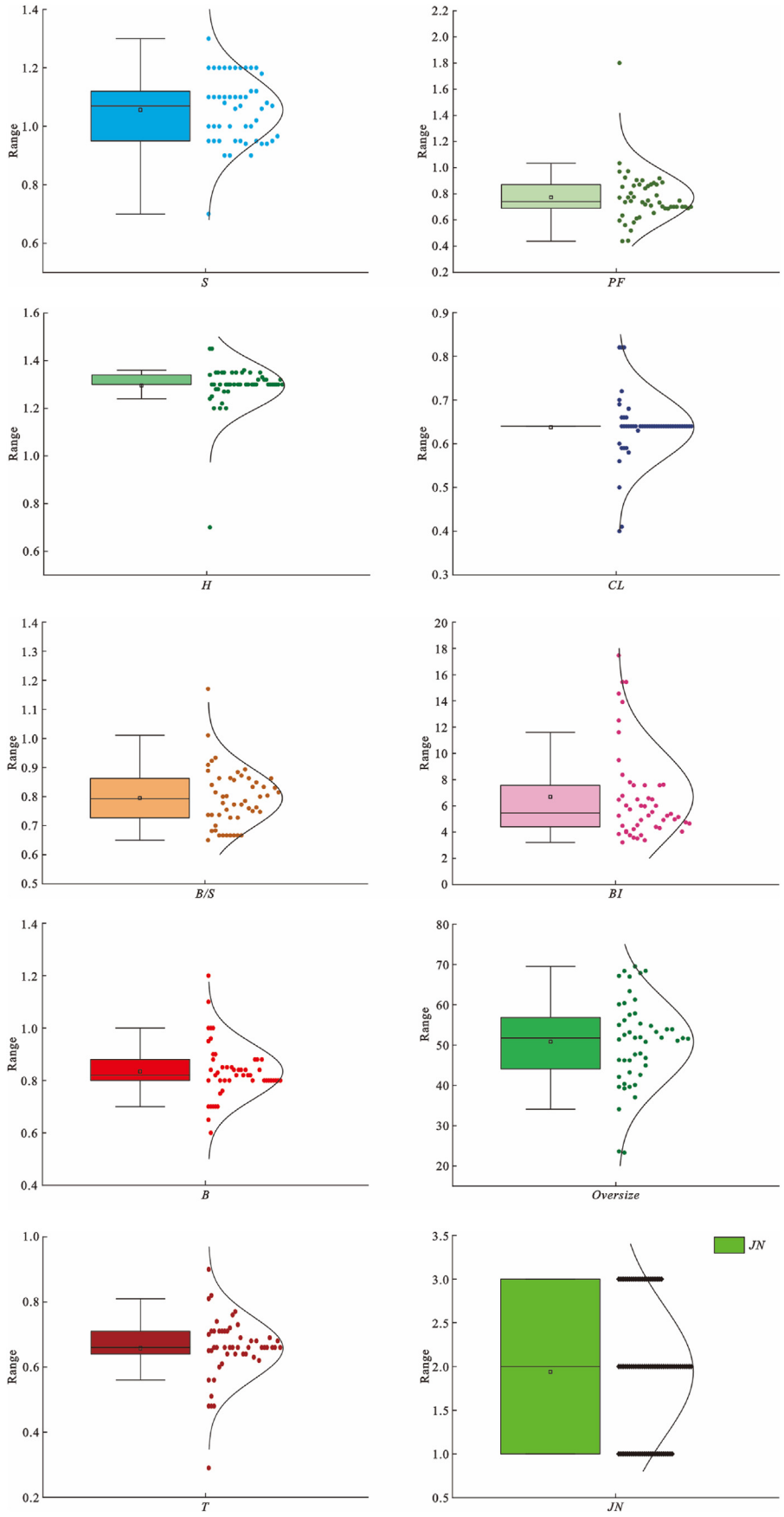


**Fig. 4.** Range value of the input and output parameters.

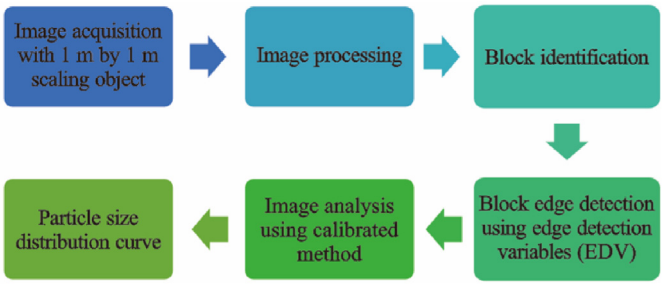


**Fig. 5.** Blast image analysis process on WipFrag 4 software [5].

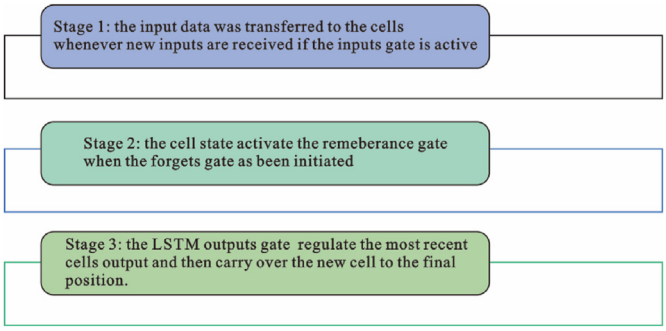


**Fig. 6.** LSTM model processing sequence.

long-short-term memory network (LSTM) is a type of recurrent neural network (RNN) that can solve issues with both long-term and short-term dependencies. Morgenroth et al. [59] used LSTM to predict a stress model update for the assessment of seismic risk at Garson Mine. The findings demonstrated good prediction accuracy (primary stresses and a six-component stress tensor) according to evaluations utilizing the Akaike information criterion (AICc), coefficient of determination (R2), and percent capture (%C) for the two input parameters anticipated. LSTM is used to anticipate the supplied data set and blast fragmentation with a step size learning rate of 0.1, a decay constant of 0.9, a momentum constant of 0.0, and an epsilon constant of 1 e−10. Four active hidden nodes, three active context nodes, and one layer were used to construct the proposed blast oversize prediction model. The suggested LSTM model was created using a deep learning MATLAB tool, and the sequence is shown in Fig. 6.

#### 4.1.1. *LSTM model development for the prediction of blast oversize*

The weight vector (*W*) and bias term (*b*), which are used to generate the controllable and uncontrolled parameters of the blast, are calculated as a vector x for the LSTM's input before being filtered by the activation function. The result will be a vector of real values between 0 and 1 as contain in Eq. (2).

$$g(x) = d(Wx + b) \tag{2}$$

For evaluating weight performance, the LSTM hidden layer gate used a sigmoid function in the range of (0,1). It multiplies the input vector by the gate's output to calculate how much information should be passed through [60]. The gate is closed when the gate output is 0, since the product result with the input vector is 0, and the information cannot pass, during the training process, the output gate value is read from 1 to 0. When the output is 1, the gate is open and the input vector is unaffected. The gate is always partially open because of the sigmoid function's range property. The unit state represented by "c" is managed by LSTM using an input gate and a forget gate. How much of the unit state "ct-1" from the prior time is still present now is determined by the forget gate. The input gate controls how much of the network's input is saved in the unit state at any one time [61]. The amount of the unit status (ct) that is output to the

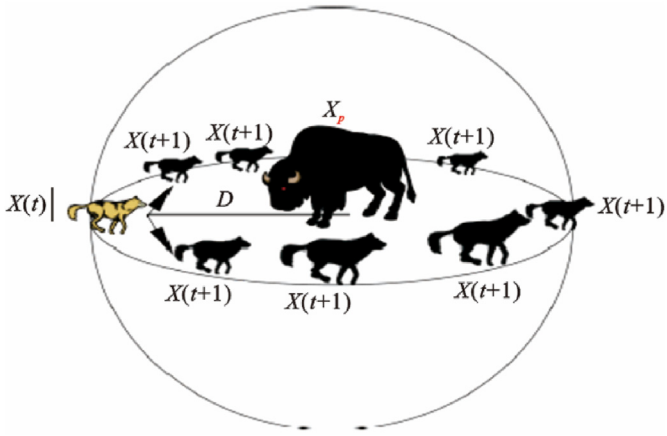


**Fig. 7.** GWO algorithm illustration [63].

LSTM's current output is controlled by output gates. The issue of vanishing gradients was solved in this study by doing numerous calculations on three gates using the Gray Wolf Optimizer, Particle Swarm Optimizer, and LSTM-TSA. As a result, the LSTM model may process input over a long period of time without experiencing gradient disappearance and yet achieve good convergence.

#### 4.1.1.1. *Hybrid LSTM with gray wolf optimizer.*

The gray wolf optimizer (GWO) is a more contemporary metaheuristic swarm intelligence approach. Mirjalili et al. [62] developed a novel model algorithm optimizer known as the Gray Wolf Optimizer (GWO) algorithm in 2014, inspired by the way timber or gray wolves hunt. The program simulates the social hierarchy of wolves. In this system, the wolves are divided into three groups (the alpha, beta, and delta groups). The alpha wolves lead the pack and make decisions, while the beta wolves support the alpha wolves' actions (Fig. 7). The delta wolves are the subordinates of the alpha and beta wolves. The circling of their prey begins the hunting staging phase. Eqs. (3)–(7) contain the algorithm for circling expressions.

The wolf positioning is represented by Eq. (3)

$$X(t+1) = X_p(t) + A \times D \tag{3}$$

$$D = \left| c \times X_p(t+1) - X_p(t) \right| \tag{4}$$

$$A = 2 \times a \times r_1 - a \tag{5}$$

$$C = 2 \times r_2 \tag{6}$$

$$a = 2 - t\left(\frac{2}{NT}\right) \tag{7}$$

where $A$ is the iteration number ranging from 0 to 2, $NT$ is the total number of iterations, $r_1$ and $r_2$ are randomly selected vectors ranging between [0,1] for the hunting process simulation, $X$ is the gray wolf position, t is the number of iterations, $X_p$ is the prey position, and finally, $D$ and $A$ can be calculated using (4) and (5). At every position taken by the wolves, there is best prey position that gives the best hunting result called best solutions as indicated in Eq. (8).

$$X(t+1) = (X_1 + X_2 + X_2) / 3 \tag{8}$$

The position of each prey within the space field ($X_2$, $X_2$, $X_2$) are computed using Eqs. (9–11) respectively.

$$X_1 = [X_\alpha - A_1 \times D_\alpha] \tag{9}$$

$$X_2 = [X_\beta - A_2 \times D_\beta] \tag{10}$$

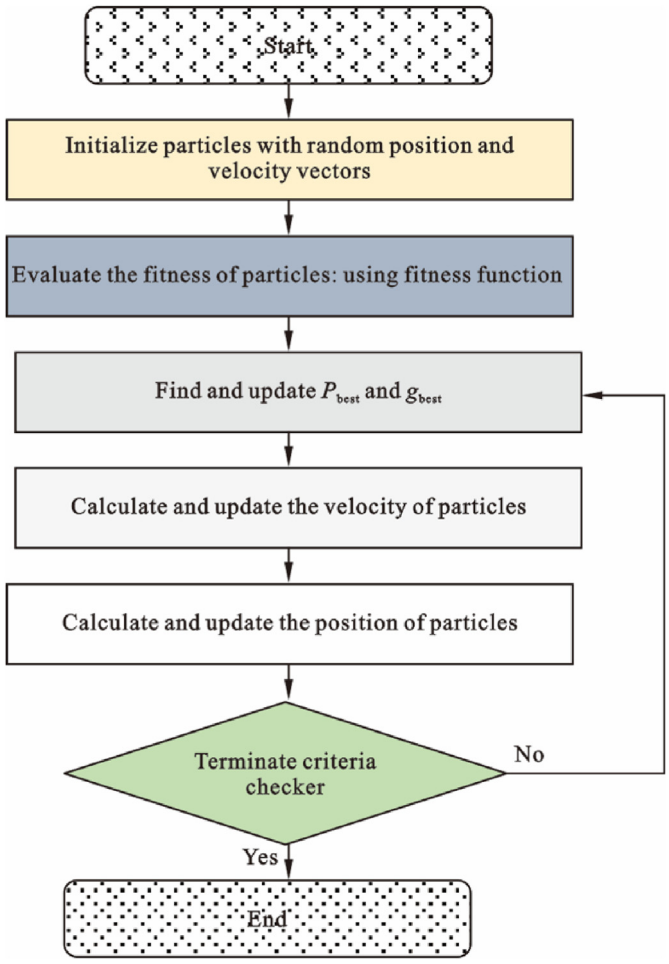


**Fig. 8.** Standard PSO flow chart (modified based on [67]).

$$X_3 = [X_\delta - A_3 \times D_\delta] \tag{11}$$

*4.1.1.2. Hybrid LSTM with particle swarm optimizer.* Eberhart and Kennedy developed Particle Swarm Optimization (PSO) [64], a parallel computational evolutionary technique, in 1995. PSO is a stochastic population-based problem-solving and solution optimization evolutionary method. It is a form of social behaviour-based avian swarm intelligence technique that can be used to help engineer applications. PSO is always moving closer to the ideal positions. However, when it approaches the global optimum, the speed of convergence slows [65]. To improve PSO performance, numerous strategies for changing the inertial weight factor are available [66]. In this study, a hybrid LSTM-PSO was developed to improve weight vector updating by decreasing error by half when compared to training the LSTM alone. During the initial stage of LSTM-PSO training, a random pattern of individuals, also known as particles, is inserted in the search area. Each particle indicates a potentially viable solution. An objective function determines the swarm's aim, with the associated value of the objective function for each particle determining its fitness. After assessing the swarm's fitness, the Eq. (12) function determines the velocities of all particles based on the best placements of the swarm and each particle. The next position of each particle is then computed using Eq. (13), which represents particle velocities. This process iterates until the swarm's termination criteria are met. These criteria could be based on the number of iterations, a specific level of accuracy, or both. Fig. 8 depicts the PSO general sequence utilized in this study to optimize the LSTM model.

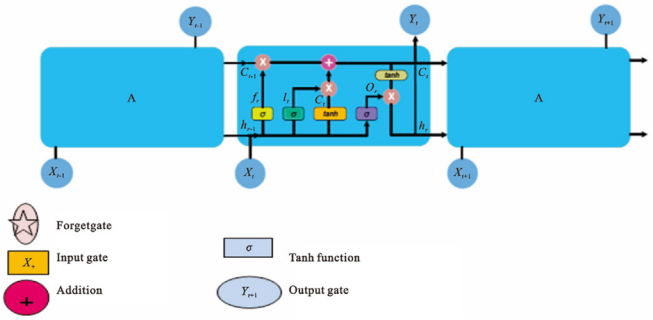


**Fig. 9.** LSTM internal structure schematic diagram.

$$\overrightarrow{Vnew} = \overrightarrow{v} + C_1 \times \left(\overrightarrow{pbest} - \overrightarrow{p}\right) + C_2 \times \left(\overrightarrow{gbest} - \overrightarrow{p}\right) \tag{12}$$

$$\overrightarrow{pnew} = \overrightarrow{v} - vnew \tag{13}$$

where *C1* and *C2* are the pre-defined coefficients; $\overrightarrow{vnew}$ , $\overrightarrow{v}$ , $\overrightarrow{pnew}$ and $\overrightarrow{p}$ are new velocity, current velocity, new position and current position of particles, respectively; $\overrightarrow{pbest}$ is the personal best position of a particle; and $\overrightarrow{gbest}$ is the global best position among all particles.

*4.1.1.3. Tree seeds algorithm-based LSTM (LSTM-TSA).* As a variant of recurrent neural networks (RNN), LSTM was created to address gradient vanishing and explosion issues that typically occur when training regular RNNs for prediction or classification challenges [68]. Except for the input and output layers, the usual deep LSTM design consists of numerous hidden layers, including LSTM layers and a fully linked layer. RNN methods contain an input gate, an output gate, and a forget gate for the purpose of generating recurrent neural networks, as depicted in Fig. 9.

In a typical LSTM cell state $C_t$, both sigmoidal layer function $\sigma$ and a pointwise multiplication operator are incorporated to control the network information through the three processing gates (forget, input, and output gates). After each state, a new data $x_t$ is sent to the network at each time instant $t$ at every instant, the decision to keep or cancel the processed information before proceeding to the memory block output $h_{t-1}$ is made in the forget gate $f_t$.

Eq. (14) is used to compute the output of the forget gate $f_t$ for each cell state.

$$f_t = \sigma\left(W_f h_{t-1} + W_f h_t + b_f\right) \tag{14}$$

where $W_f$ and $W_f$ rare the input weight and bias of the forget gate respectively.

Eq. (15) represent the input gate computational equation to determine whether $x_t$ will be stored in the cell state $c_t$.

$$i_t = \sigma(W_i h_{t-1} + W_i h_t + b_i) \tag{15}$$

where $i_t$ is the input gate; $W_i$ and $b_i$ are the input weight and bias of the input gate, respectively.

A new vector $\tilde{C}_t$ is generated using tanh layer function as expressed in Eq. (16) to introduce the cell state $C_t$ process stage condition.

$$\tilde{C}_t = tan\, h(W_c h_{t-1} * W_c x_t * b_c) \tag{16}$$

where $W_c$ is the cell state weight; $b_c$ is the cell state bias; and * is the Hadamard product [69].

The model output memory block $h_t$ in Fig. 9 is created by using the output gate $o_t$ and another tanh layer, as express in Eqs. (17) and (18).

$$o_t = \sigma(W_o h_{t-1} + W_o x_t + b_o \tag{17}$$

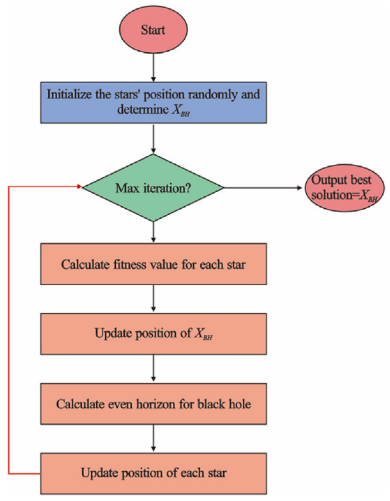


**Fig. 10.** Flowchart of the BHA algorithm.

$$h_t = o_t * \tanh(c_t) \tag{18}$$

where $h_t$ and $h_t$ are the input weight and bias of the output gate.

LSTM and TSA can effectively predict rock fragment size distribution post-blasting due to their capacity to analyse sequential data. LSTM's memory cells enable learning from past observations while TSA recognizes temporal trends. These techniques consider factors like explosive type, rock properties, and blast parameters, crucial for accurate predictions. Their adaptability to handle time-series data and capture complex relationships make them robust tools for forecasting the intricate dynamics of rock fragmentation following blasting operations.

*4.1.1.4. Hybrid LSTM with black hole optimization algorithm.* The Black hole optimization algorithm (BHA) is a swarm-based searching technique that attempts to replicate the phenomena of black holes seen throughout the cosmos. An area in universe that has a very high concentration of mass is known as a black hole (BH). The singularity, also called as the core of the BH, is where all particle mass is concentrated. Every neighbouring particle is kept in place by what is known as events horizon, which is a powerful gravity attraction that surrounds the black hole singularity and prohibits them from escaping [70].

In the BHA, each solution is referred to as a star, thus the process starts by randomly constructing the stars in the searching spaces. This is performed such that it can identify the optimal solution. Subsequently, it analyses each star to locate the optimum solution, which is referred to as BH. The stars continue travelling along the direction of the BH, and as a result, the BH begins absorbing them. Eq. (19) describes how the motion of the stars is accomplished:

$$x^i(t+1) = x^i(t) + r[x_{BH} - x^i(t)] \tag{19}$$

where $x^i(t)$ and $x^i(t+1)$ are the locations of the $i_{th}$ star at repetitions $t$ and $t+1$, respectively; $r$ is a random value between (0, 1); and $x_{BH}$ is the location of the BH in searching spaces.

The BHA can choose the location of a star as the BH if that star travels closer to the BH and achieves a superior location along the way. Meanwhile, the BH adjusts its location and travels to where the star is located once it has updated its position. In addition, when a star travels over the events horizon of the BH while it is in motion, the BH will consume the star and produce a newborn star by a randomized process. Whenever the distance between the star and the black hole is smaller than the radius of the event horizon, the star is removed from the universe solution. Eq. (20) can be used to determine the radius of the event horizon, denoted by $R$.

$$R = \frac{f_{BH}}{\sum_{i=1}^{n} f_i} \tag{20}$$

where $f_{BH}$ is the fitness value of each BH; $f_i$ is the fitness value of the $i_{th}$ star; and $n$ is the population size (total number of stars).

The algorithm shall keep running until a certain level of repetitions has been reached. The flow chart for the BHA is shown in Fig. 10. As the BHA discovers a new star in the searching spaces, the algorithm instantly evaluates that star to see whether it satisfies the criteria for fitness. If the fitness value of the new star is higher than that of the BH, the algorithm will replace the BH with the newborn star before moving on to the stage when it updates the location of the star. The BHA's exceptional benefits over other nature-inspired optimization algorithms, such as strong capacity in avoiding local optima, rapid convergences, simple, and parameter-free construction, led us to apply it in picture improvement [71]. BHA achieves better performance than other optimization approaches for a variety of issues; however, it does not have enough exploration abilities for particular dataset.

## 5. Model development

### 5.1. Hybrid LSTM models

In this work, a new LSTM intelligent optimizer based on the relationship between trees and their seeds was applied for continuous optimization. The new LSTM hybrid technique falls within the categories of heuristic and population-based search. When utilizing TSA, the position of trees and seeds in n-dimensional search space corresponds to the likely solution of an optimization issue. The trees produce one or more seeds, and the better seed placements are replaced by fresh tree placements. When producing new seed locations, either the ideal option or another tree site for the tree location is considered. In research, the usage of a tree-based algorithm (TSA) has gained traction. Kiran [72] used the TSA iteration technique to solve optimization problems. Ding et al. [73] employed the tree-seed method (TSA) to find structural systems and nonlinear hysteretic parameters. The tree-seed algorithm approach was applied to the LSTM algorithm in this work to improve the nonlinearity of the various gate parameters. The regression graphs for the proposed LSTM-TSA, LSTM-PSO, LSTM-GWO, and LSTM models are also displayed in Fig. 11. Fig. 11 shows that the coefficient of determination ($R^2$) values obtained during model training are greater than 95 %. The proposed LSTM models can thus properly forecast the blast oversize percentage. Tables 3 show the estimated blast oversize and $R^2$ values for the four LSTM models.

### 5.2. RF model for the predictions of blast oversize

Random forest (RF) is a well-known and basic machine learning technique based on ensemble learning that integrates many classifiers to construct a powerful model, according to Kapucu and Cubukcu [74]. Classification and regression concerns can be overcome using RF, a high-accuracy supervised machine learning technique [75,76]. RF has not been used to estimate how blast production will affect downstream operations [77]. To improve the TBM's penetration and drilling performance, Kong et al. [76] employed RF to forecast the thrust and torque of an earth pressure balance shield TBM in a soil-rock mixed-face terrain. Their findings show that the RF method was more exact than theoretical models. The RF modeling approach has frequently been used in mining engineering to address classification and regression problems [78–81]. Random forests are constructed for this study's oversize percentage prediction by building trees based on a random vector so that the tree predictor takes on numerical values rather than class labels. The regression graphs of the proposed RF model for the train and test datasets are shown in Fig. 12. The graph shows that the coefficients of determination ($R^2$) values for the model's training and testing datasets are greater than 98 %

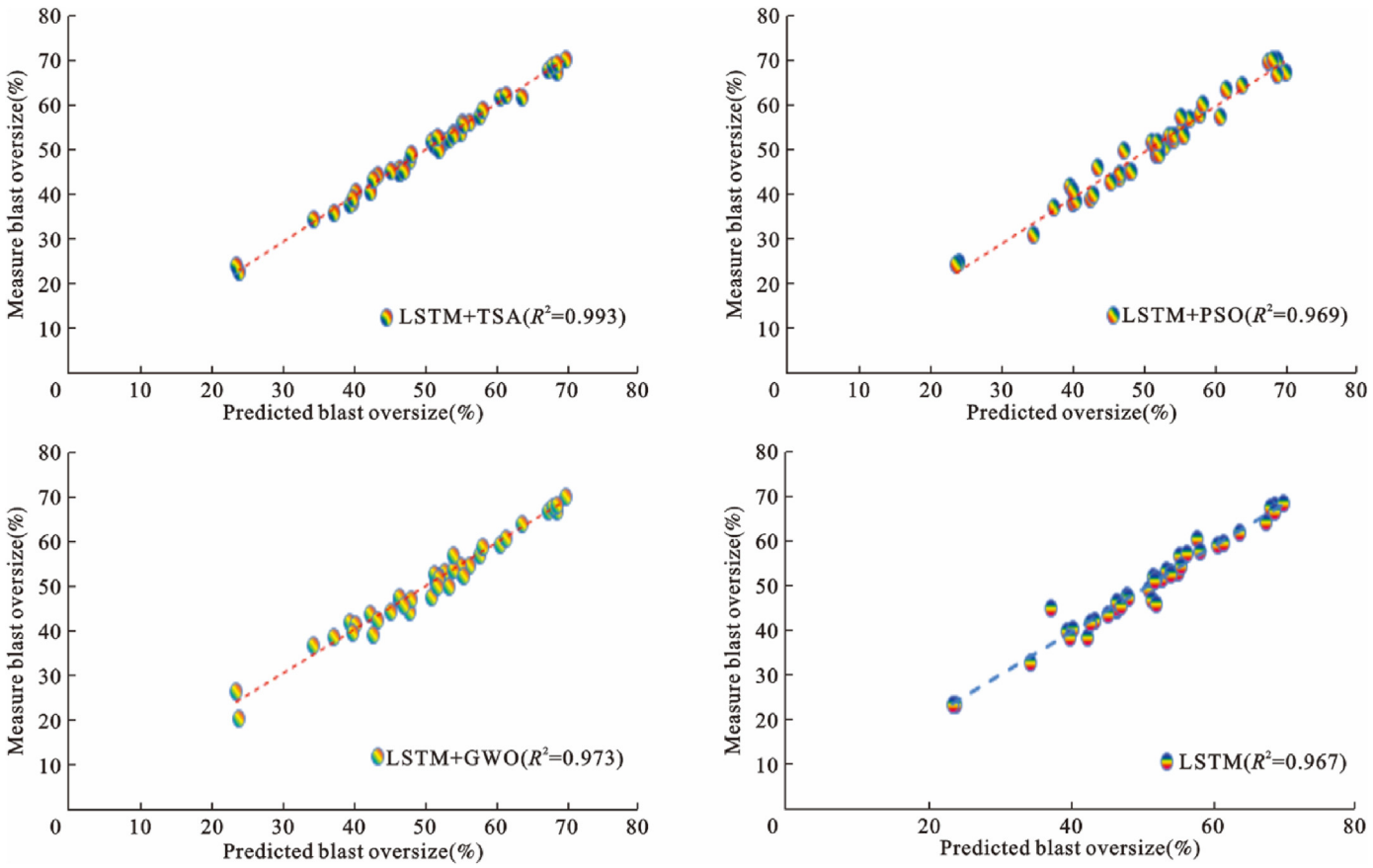


**Fig. 11.** Relationship between the measured and LSTM, Hybrid LSTM predicted oversize.

**Table 3**
Prediction Result of LSTM, Hybrid LSTM for the test data.

| Data ID | TD-1 | TD-2 | TD-3 | TD-4 | TD-5 | TD-6 | TD-7 | TD-8 |
|---|---|---|---|---|---|---|---|---|
| Measured oversize | 53.18 | 51.8 | 51.94 | 66.98 | 27.34 | 54.81 | 40.35 | 60.11 |
| LSTM ($R^2$ = 0.945) | 55.34 | 59.29 | 53.06 | 68.98 | 25.19 | 58.59 | 44.52 | 58.52 |
| LSTM + PSO ($R^2$ = 0.946) | 50.37 | 55.67 | 55.61 | 66.38 | 30.06 | 54.64 | 37.12 | 63.02 |
| LSTM + GWO ($R^2$ = 0.953) | 52.78 | 51.66 | 54.34 | 64.9 | 24.03 | 54.25 | 43.84 | 55.89 |
| LSTM + TSA ($R^2$ = 0.983) | 51.66 | 52.81 | 52.26 | 62.71 | 28.13 | 51.39 | 41.02 | 58.29 |

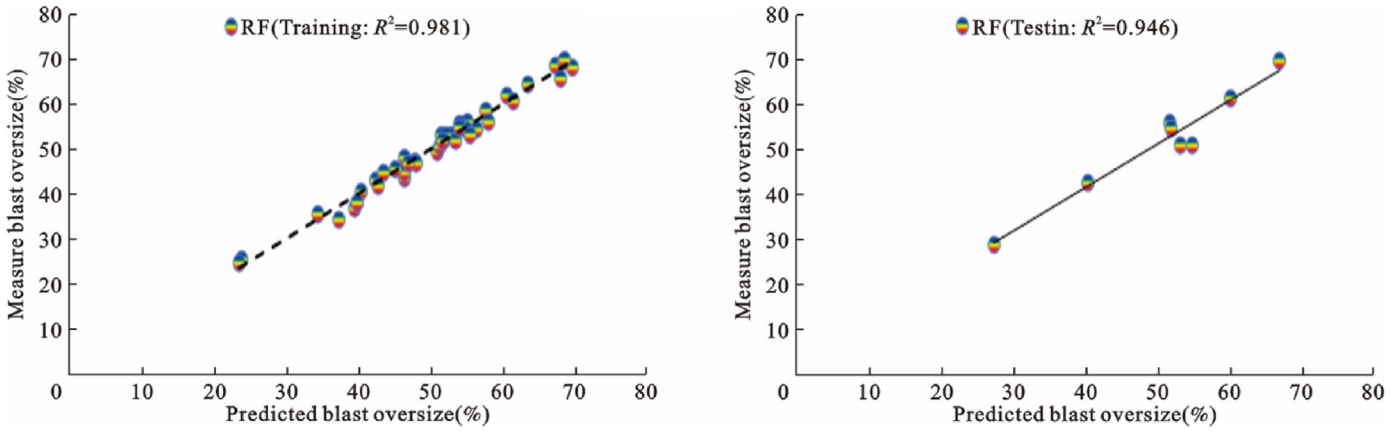


**Fig. 12.** Relationship between the RF predicted Oversize and measured values.

and 94 %, respectively. As a result, the proposed RF model can accurately estimate the blast oversize percentage.

### *5.3. SVR models for the predictions of blast oversize*

SVM is built on Kernel functions and decreases architectural risk by

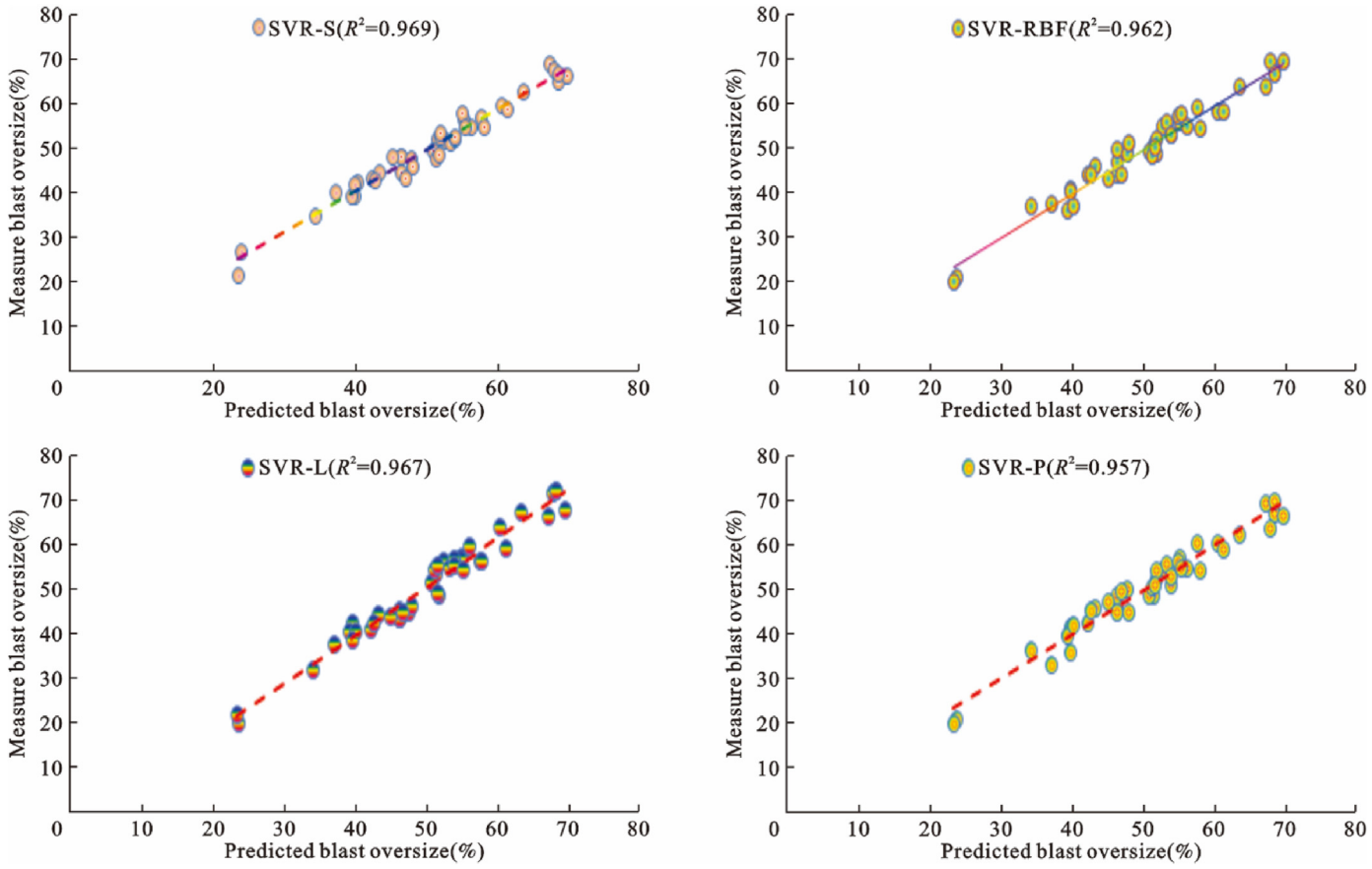


**Fig. 13.** Relationship between the SVR predicted oversize and measured values.

reducing overfitting with regularization settings [82]. Longjun et al. [83] discussed the distinctions between SVM and other machine learning approaches. The support vector machine (SVM) is a relatively new research approach. It is a machine learning theory framework with a wide approach based on statistics theory that was built using a set of finite samples. This method has gotten a lot of attention because of its improved performance when applied to real-world problems like small sample sizes, nonlinear analysis, and local minimum points. In this study, multiple kernels, including the spline kernel (SVR-S), the Gaussian-RBF kernel (SVR-RBF), the linear Kernel (SVR-L), and the polynomial Kernel (SVR-P), were built utilizing the SVR architecture, which stands for insensitive SVR. The regression graphs for the suggested SVR-S, SVR-RBF, SVR-L, and SVR-P models are also shown in Fig. 13. Fig. 13 shows that the coefficient of determination ($R^2$) values obtained during model training are greater than 95 %. The proposed LSTM models can thus properly forecast the blast oversize percentage. Tables 4 show the anticipated blast oversize and $R^2$ values for each of the four LSTM models.

## 6. Results and discussion

### 6.1. Model comparison

SVR and RF models were compared to models developed in the proposed study for blast oversize percentage prediction using hybrid LSTM. Table 5 and Fig. 14 show the coefficient of determination rankings for all of the developed models. The ranking study demonstrates that LSTM-TSA is more accurate than other hybrid LSTM, RF, and SVR models (with $R^2 = 0.993$ for the training dataset and $R^2 = 0.983$ for the testing dataset). In terms of blast oversize predictions, the proposed models outperform the PSO and GWO hybrid models, SVR, and RF models examined in this work.

### 6.2. Model error analysis result

The performance of the proposed models was evaluated using three forms of estimating errors: mean absolute error (MAE), root mean square error (RMSE), and value account factor (VAF). The RMSE error analysis index assesses the difference between measured and expected values to

**Table 4**
Prediction result of different Kernel modified SVR (KM-SVR) for the test data.

| Data ID | TD-1 | TD-2 | TD-3 | TD-4 | TD-5 | TD-6 | TD-7 | TD-8 |
|---|---|---|---|---|---|---|---|---|
| Oversize | 53.18 | 51.8 | 51.94 | 66.98 | 27.34 | 54.81 | 40.350 | 60.110 |
| SVR-L ($R^2 = 0.933$) | 49.42 | 52.04 | 49.72 | 65.56 | 31.47 | 60.38 | 43.3 | 60.74 |
| SVR-P ($R^2 = 0.948$) | 52.65 | 53.86 | 46.63 | 66.49 | 22.65 | 49.5 | 40.87 | 62.96 |
| SVR-S ($R^2 = 0.945$) | 56.47 | 48.24 | 56.47 | 63.9 | 24.06 | 53.42 | 39.62 | 59.00 |
| SVR-RBF ($R^2 = 0.952$) | 52.44 | 50.72 | 53.15 | 72.75 | 30.37 | 61.29 | 38.85 | 65.7 |

**Table 5**
Model ranking analysis result.

| Model | $R^2$ of train | $R^2$ of test | Rate | Rate | Sum | Rank |
|---|---|---|---|---|---|---|
| LSTM | 0.9668 | 0.9453 | 3 | 3 | 6 | 8 |
| LSTM + PSO | 0.9685 | 0.9457 | 5 | 4 | 9 | 4 |
| LSTM + GWO | 0.9725 | 0.9531 | 7 | 8 | 15 | 2 |
| LSTM + TSA | 0.9931 | 0.9832 | 9 | 9 | 18 | 1 |
| SVR-L | 0.9674 | 0.9328 | 4 | 1 | 5 | 9 |
| SVR-P | 0.9568 | 0.9481 | 1 | 6 | 7 | 7 |
| SVR-S | 0.9686 | 0.9448 | 6 | 2 | 8 | 6 |
| SVR-RBF | 0.9623 | 0.9518 | 2 | 7 | 9 | 4 |
| RF | 0.9812 | 0.946 | 8 | 5 | 13 | 3 |

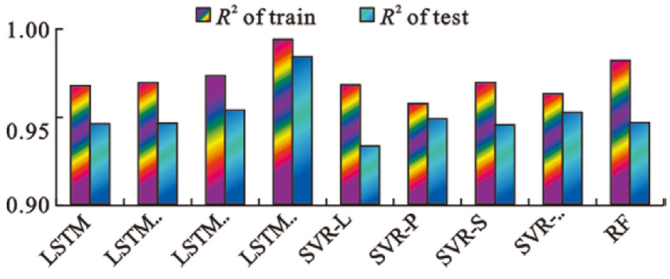


**Fig. 14.** Comparison of model coefficient of determination.

determine how well predicted and measured values fit together. The expression required to calculate RSME is given in Eq. (21).

$$\mathrm{RMSE} = \sqrt{\frac{\sum_{i=1}^{N}(Mi - Pi)^2}{N}} \tag{21}$$

Using Eq. (22), the mean absolute error of each model's predicted values relative to the measured values was assessed. The link between the predictive value and the measured value is accurately represented by MAE.

$$\mathrm{MAE} = \frac{1}{N}\sum_{i=1}^{N} /Ai - Pi/ \tag{22}$$

Value account for error index was calculated in this study using Eq. (23) with the predicted value and measure value as the input data element.

$$\mathrm{VAF} = \left[1 - \frac{Var(Mi - Pi)}{var(Mi)}\right] \times 100 \tag{23}$$

where $N$ is the total number of blast data; $P_i$ is the predicted value; and $M_i$ is the measure blast oversize percentage values.

The lower the amount of the root mean square error, the greater the mean absolute error, and the greater the VAF, the better the model's prediction ability. Similarly, value account for displays the discrepancy between the expected and measured value on-site. Table 6 shows the error analysis performed in this investigation.

The MAE, RSME and VAF for both the ordinary LSTM and RF show least error follow by LSTM-GWO. Similarly, SVR-L and SVR-P model has the highest error values follow by LSTM-PSO model and then SVR-RBF model. In this study, the three-error analysis shows that LSTM-TSA has the best fitting for the prediction of blast oversize prediction with the lowest RSME, and MAE and the highest VAF values for both training and testing dataset as shown in Fig. 15. Hence, the performance of the proposed models is promising. In this study, the TSA-based LSTM presented better overall performance than none-optimized LSTM and other optimized LSTM as well as RF and SVRs, it is due to that the TSA can help procure better hyper-parameters in LSTM and thus generate better prediction model. For the RF, it might be more suited for tabular data with structured features and for the SVRs, it works well for high-dimensional

**Table 6**
Error analysis results.

| Metric | MAE | | RMSE | | VAF | |
|---|---|---|---|---|---|---|
| Model | Train | Test | Train | Test | Train | Test |
| LSTM | 1.1871 | 3.0575 | 1.9650 | 3.6202 | 96.6768 | 93.3331 |
| LSTM + PSO | 1.7831 | 2.4975 | 2.0000 | 2.8069 | 96.5882 | 94.3828 |
| LSTM + GWO | 1.4498 | 2.0750 | 1.7921 | 2.5378 | 97.2454 | 95.2891 |
| LSTM + TSA | 0.8755 | 1.7275 | 0.9712 | 2.1722 | 99.2131 | 97.1649 |
| SVR-L | 2.0736 | 2.6150 | 2.2854 | 3.1289 | 95.5045 | 92.8650 |
| SVR-P | 2.0802 | 2.7200 | 2.3372 | 3.3828 | 95.5192 | 92.5690 |
| SVR-S | 1.6536 | 2.6213 | 1.9560 | 2.9146 | 96.7209 | 93.7593 |
| SVR-RBF | 1.9093 | 3.1750 | 2.1471 | 3.8913 | 96.0951 | 92.5250 |
| RF | 1.3729 | 2.6050 | 1.5053 | 2.7977 | 98.0830 | 94.5095 |

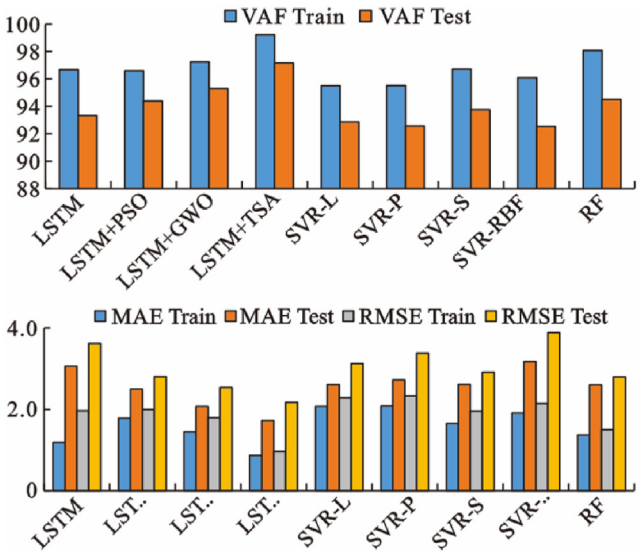


**Fig. 15.** Relation between the error indices for all the developed models.

data. However, it should be noted that LSTM, RF, and SVR are different types of machine learning models, each with its own strengths and weaknesses. The choice between them depends largely on the specific problem that we want to solve.

### 6.3. Input variable impact on the model output

Sensitivity analysis is a technique for determining which input parameters have the greatest influence on model output parameters. The results of the SHAP (Shapley additive explanation) and Moris sensitivity analyses performed in this work to assess the sensitivity of all input

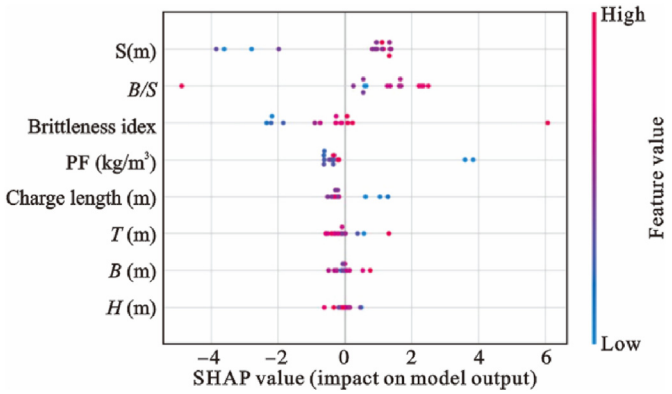


**Fig. 16.** SHAP additive for selection of feature importance from the variables.

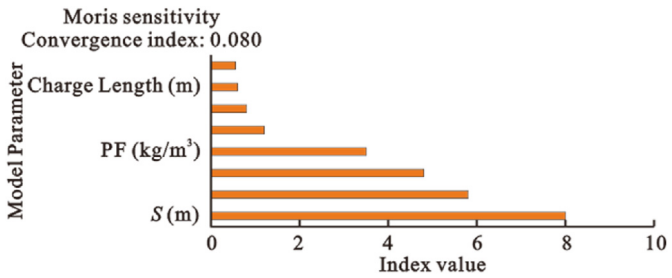


**Fig. 17.** Moris analysis result for the model inputs.

**Table 7**
Comparison of primary crusher stats before and after LSTM application.

| Blast design | | | Primary crusher statistics | |
|---|---|---|---|---|
| Item | Before | After | | |
| *B* (m) | 1.2 | 0.7 | Productivity (ton/h) | |
| *S* (m) | 1.3 | 0.9 | Before | After |
| *T* (m) | 0.9 | 0.65 | 16 (ton/h) | 20.5 (ton/h) |
| *H* (m) | 1.45 | 1.4 | | |
| *CL* (kg) | 0.82 | 0.7 | | |
| *PF* (kg/m$^3$) | 1.8 | 1.03 | | |
| Oversize (%) | 50.82 | 35 | | |

variables on blast fragmentation oversize percent are shown in Figs. 16 and 17. Several scholars in the field of rock mechanics have employed the SHAP analysis method. Fissha et al. [84] investigated the effect of several parameters on blast-induced ground vibration. As a result, a SHAP and Moris sensitivity analysis was performed in this study using the percentage oversize and the order of importance of the independent variables. For each model generated, the results reveal the strength of the relationship between the input and output parameters. The analysis results revealed that, the spacing distance has the greatest influence on blast percentage oversize, followed by the brittleness index, burden to spacing ratio, and powder factor.

### *6.4. Comparison of primary crusher stats before and after LSTM application*

The blast inputs and equipment data in Table 7 show a considerable improvement when the input blast parameters were simulated using the LSTM-TSA model prior to blasting. The simulated blast result was within the company's guidelines. The proportion of big rock fragments was reduced from 50.83 % to 35 %, which was within the specified limit. The simulated blast parameters improved the crusher's productivity by 28.1 %.

## 7. Conclusions

To optimize downstream operations, the generation of boulders stands as a critical factor demanding attention. In this current study, a novel hybrid model is devised, integrating geological and blast-based inputs, with the aim of achieving precision in predicting boulder sizes. Unlike conventional data loading approaches, the model considers rock joints alongside other blast design parameters, enhancing predictive accuracy. Consequently, three comprehensive combinational models—LSTM, SVR, and RF—are meticulously developed utilizing fifty blast dataset entries, aiming to accurately predict rock boulder dimensions. The proposed models were assessed using root mean square error (RSME), variance accounted for (VAF), and mean absolute error (MAE) to gauge prediction accuracy. This comparison aimed to evaluate model performance. Subsequently, SHAP was employed to analyse each input parameter's impact on the model's output. The study scrutinized the efficacy of multiple models, with the LSTM-TSA model emerging as the top performer, surpassing the gray wolf-optimized LSTM, SVR-S, SVR-L, and RF models. Following closely were the LSTM-PSO and RF models. Despite variations, all models demonstrated satisfactory performance suitable for real-world applications. The LSTM-TSA soft computing model was specifically leveraged to optimize various blast parameters such as burden, spacing, stemming length, drill hole length, charge length, powder factor, and joint set number. The estimated percentage oversize values for these parameters were determined as 0.7, 0.9, 0.65, 1.4, 0.7 m, 1.03 kg/m$^3$, 35 %, and 2, respectively. Additionally, the models underwent scrutiny through SHAP and Moris sensitivity analysis to ascertain feature importance and augment their practicality. For industrial application, the influential factors as used in this study can be considered as inputs and the optimized blasting boulder size would be obtained to predict a pre-optimized blasting design. As a result, the risk of over-sized blasting boulders would be reduced and also provide a more reasonable blasting design. In addition, the optimized LSTM model can be considered to be used for software development of blasting design and provide a fast blasting design scenario for mining workers.

The future work will be focused on applying numerical modelling techniques such as LS-DYNA, universal discrete element continua (UDEC) and Fast Lagrangian Analysis of Continua (FLAC) in modelling the effect of geological properties and rock chemical composition on explosive efficiency. And then, more advanced regression techniques, optimization algorithms and deep learning techniques are worthwhile to be used and compared with the proposed methods in this study, such as salp swarm algorithms [85,86], convolutional neural network [21,87], extreme gradient boosting [88] and extreme learning machine [23].

## Declaration of conflict of interest

The authors declare the following financial interests/personal relationships which maybe considered as potential competing interests. Blessing Olamide TaiwoJ is currently employed by HNF Global Resources Limited, Akoko Edo, Nigeria. N. Sri Chandrahas is currentlu employed by Mine Planning Division, GMMCO Technology Services (GTS), Hyderabad, 500008, India

## Acknowledgements

This study is funded by China Scholarship Council (No.202006370006).

## References

[1] D. Ramesh, N.S. Chandrahas, M.S. Venkatramayya, M. Naresh, P. Talari, D.U.V.D. Prasad, et al., Effects of spacing-to-burden ratio and joint angle on rock fragmentation: an unmanned aerial vehicle and AI approach in overburden benches, ATG 2 (2023) 155–166.
[2] N.S. Chandrahas, B.S. Choudhary, M.S. Venkataramayya, Competitive algorithm to balance and predict blasting outcomes using measured field data sets, Comput. Geosci. 27 (2023) 1087–1110.
[3] T.M. Klapötke, Chemistry of High-Energy Materials, De Gruyter, 2022.
[4] S.P. Singh, R. Narendrula, Causes, implications and control of oversize during blasting, in: Proceedings of the 9th International Symposium on Rock Fragmentation by Blasting, 2009, pp. 311–317. Granada, Spain.
[5] N.S. Chandrahas, Y. Fissha, B.S. Choudhary, B. Olamide Taiwo, M.S. Venkataramayya, T. Adachi, Experimental data – driven algorithm to predict muckpile characteristics in jointed overburden bench using unmanned aerial vehicle and AI tools, Int. J. Min. Reclamat. Environ. (2024) 1–35.
[6] C. Joshua, Determination of Explosive Energy Partition Values in Rock Blasting through Small-Scale Testing, Doctoral Dissertation, University of Kentucky, 2015.
[7] M. Naresh, N. Sri Chandrahas, G. Praful Kumar, T. Pradeep Kumar, K. Sravan Kumar, Harmonizing Blasting Efficiency: A Case Study on Evaluation and Optimization of Fragmentation Size and Ground Vibration, J Inst Eng India Ser D, 2024.
[8] E.M. Kinyua, Z. Jianhua, R.M. Kasomo, D. Mauti, J. Mwangangi, A review of the influence of blast fragmentation on downstream processing of metal ores, Miner. Eng. 186 (2022) 107743.
[9] E. Li, F. Yang, M. Ren, X. Zhang, J. Zhou, M. Khandelwal, Prediction of blasting mean fragment size using support vector regression combined with five optimization algorithms, J. Rock Mech. Geotech. Eng. 13 (2021) 1380–1397.

[10] N.S. Chandrahas, B.S. Choudhary, M.V. Teja, M.S. Venkataramayya, N.S.R.K. Prasad, XG boost algorithm to simultaneous prediction of rock fragmentation and induced ground vibration using unique blast data, Appl. Sci. 12 (2022) 5269.
[11] A. Al-Bakri, M. Hefni, A review of some nonexplosive alternative methods to conventional rock blasting, Open Geosci. 13 (2021) 431–442.
[12] B.O. Taiwo, Y. Fissha, T. Palangio, A. Palangio, H. Ikeda, N.R. Cheepurupalli, et al., Assessment of charge initiation techniques effect on blast fragmentation and environmental safety: an application of WipFrag software, Mining 3 (2023) 532–551.
[13] O.Y. Odeyemi, B.O. Taiwo, O. Alaba, Influence of explosive maximum instantaneous charge on blasting environmental impact, J. Sustain. Min. 22 (2023) 344–357.
[14] S. Moray, N. Throop, J. Seryak, C. Schmidt, C. Fisher, M. D'Antonio, et al., Energy efficiency opportunities in the stone and asphalt industry, in: Twenty- Eighth Industrial Energy Technology Conference, 2006, pp. 71–83.
[15] T. Norgate, N. Haque, Energy and greenhouse gas impacts of mining and mineral processing operations, J. Clean. Prod. 18 (2010) 266–274.
[16] B. Klein, C. Wang, S. Nadolski, Energy-efficient comminution: best practices and future research needs, in: K. Awuah-Offei (Ed.), Energy Efficiency in the Minerals Industry, Springer International Publishing, Cham, 2018, pp. 197–211.
[17] B. Gong, T. Zhao, I. Thusyanthan, C. Tang, Modelling rock fracturing by a novel implicit continuous to discontinuous method, Comput. Geotech. 166 (2024) 106035.
[18] X. Feng, B. Gong, Z. Liang, S. Wang, C. Tang, H. Li, et al., Study of the dynamic failure characteristics of anisotropic shales under impact Brazilian splitting, Rock Mech. Rock Eng. 57 (2024) 2213–2230.
[19] Y. Wang, B. Gong, C. Tang, X. Yang, Size effect and lateral pressure effect on the mechanical resistance of columnar jointed basalt, Int. J. Rock Mech. Min. Sci. 171 (2023) 105571.
[20] W. Zhang, X. Gu, L. Tang, Y. Yin, D. Liu, Y. Zhang, Application of machine learning, deep learning and optimization algorithms in geoengineering and geoscience: comprehensive review and future challenge, Gondwana Res. 109 (2022) 1–17.
[21] S. Liu, L. Wang, W. Zhang, W. Sun, Y. Wang, J. Liu, Physics-informed optimization for a data-driven approach in landslide susceptibility evaluation, J. Rock Mech. Geotech. Eng. (2024) S167477552400088X.
[22] E. Li, N. Zhang, B. Xi, Z. Yu, Y. Fissha, B.O. Taiwo, et al., Analysis and modelling of gas relative permeability in reservoir by hybrid KELM methods, Earth Sci. Inform. (2024).
[23] W. Zhang, X. Gu, L. Hong, L. Han, L. Wang, Comprehensive review of machine learning in geotechnical reliability analysis: algorithms, applications and further challenges, Appl. Soft Comput. 136 (2023) 110066.
[24] K. Greff, R.K. Srivastava, J. Koutnik, B.R. Steunebrink, J. Schmidhuber, LSTM: a search space odyssey, IEEE Transact. Neural Networks Learn. Syst. 28 (2017) 2222–2232.
[25] Y. Bengio, P. Simard, P. Frasconi, Learning long-term dependencies with gradient descent is difficult, IEEE Trans. Neural Network. 5 (1994) 157–166.
[26] M. Varsha, B. Poornima, H.P. Vinutha, K.M.P. Pavan, Predictive model for rice blast disease on climate data using long short-term memory and multi-layer perceptron: an empirical study on davangere district 25 (6) (2021) 4703–4722.
[27] K. Awuah-Offei, Energy efficiency in mining: a review with emphasis on the role of operators in loading and hauling operations, J. Clean. Prod. 117 (2016) 89–97.
[28] P.K. Singh, M.P. Roy, R.K. Paswan, Md Sarim, S. Kumar, R. Ranjan Jha, Rock fragmentation control in opencast blasting, J. Rock Mech. Geotech. Eng. 8 (2016) 225–237.
[29] K. Awuah-Offei (Ed.), Energy Efficiency in the Minerals Industry, Springer International Publishing, Cham, 2018.
[30] S.V. Manyele, Investigation of excavator performance factors in an open-pit mine using loading cycle time, Engineering 9 (2017) 599–624.
[31] H. Moomivand, H. Amini Khoshalan, J. Shakeri, H. Vandyousefi, Development of new comprehensive relations to assess rock fragmentation by blasting for different open pit mines using GEP algorithm and MLR procedure, Int. J. Min. Geol. Eng. (2022).
[32] M. Danielsson, E. Söderström, H. Schunnesson, A. Gustafson, H. Fredriksson, D. Johansson, et al., Predicting rock fragmentation based on drill monitoring: a case study from Malmberget mine, Sweden, J. S. Afr. Inst. Min. Metall 122 (2022) 1–11.
[33] Z. Jia, Z. Song, J. Fan, J. Jiang, Prediction of blasting fragmentation based on GWO-ELM, Shock Vib. 2022 (2022) 1–8.
[34] R. Amoako, A. Jha, S. Zhong, Rock fragmentation prediction using an artificial neural network and support vector regression hybrid approach, Mining 2 (2022) 233–247.
[35] B.O. Taiwo, Effect of charge load proportion and blast controllable factor design on blast fragment size distribution, J. Brilli. Eng. 3 (2022) 1–6.
[36] C. Grundstrom, S. Kanchibotla, A. Jankovich, D. Thornton, D.D.N.A. Pacific, Blast fragmentation for maximising the sag mill throughput at Porgera Gold Mine, in: The annual conference on explosives and blasting technique 1, 2001, pp. 383–400.
[37] R.M. Bhatawdekar, D.J. Armaghani, A. Azizi, Review of Empirical and Intelligent Techniques for Evaluating Rock Fragmentation Induced by Blasting. Environmental Issues of Blasting, Springer Nature Singapore, Singapore, 2021, pp. 21–39.
[38] R.M. Bhatawdekar, R. Kumar, M.M. Sabri Sabri, B. Roy, E.T. Mohamad, D. Kumar, et al., Estimating flyrock distance induced due to mine blasting by extreme learning machine coupled with an equilibrium optimizer, Sustainability 15 (2023) 3265.
[39] M. Monjezi, M. Rezaei, A.Y. Varjani, Prediction of rock fragmentation due to blasting in Gol-E-Gohar iron mine using fuzzy logic, Int. J. Rock Mech. Min. Sci. 46 (2009) 1273–1280.
[40] M. Monjezi, M. Rezaei, A. Yazdian, Prediction of backbreak in open-pit blasting using fuzzy set theory, Expert Syst. Appl. (2010).
[41] A. Bahrami, M. Monjezi, K. Goshtasbi, A. Ghazvinian, Prediction of rock fragmentation due to blasting using artificial neural network, Eng. Comput. 27 (2011) 177–181.
[42] A. Sayadi, M. Monjezi, N. Talebi, M. Khandelwal, A comparative study on the application of various artificial neural networks to simultaneous prediction of rock fragmentation and backbreak, J. Rock Mech. Geotech. Eng. 5 (2013) 318–324.
[43] A. Karami, S. Afiuni-Zadeh, Sizing of rock fragmentation modeling due to bench blasting using adaptive neuro-fuzzy inference system (ANFIS), Int. J. Min. Sci. Technol. (2013).
[44] S. Shams, M. Monjezi, V.J. Majd, D.J. Armaghani, Application of fuzzy inference system for prediction of rock fragmentation induced by blasting, Arabian J. Geosci. (2015).
[45] E. Ebrahimi, M. Monjezi, M.R. Khalesi, D.J. Armaghani, Prediction and optimization of back-break and rock fragmentation using an artificial neural network and a bee colony algorithm, Bull. Eng. Geol. Environ. (2016).
[46] M. Hasanipanah, D. Jahed Armaghani, M. Monjezi, S. Shams, Risk assessment and prediction of rock fragmentation produced by blasting operation: a rock engineering system, Environ. Earth Sci. 75 (2016) 1–12.
[47] P.F. Asl, M. Monjezi, J.K. Hamidi, D.J. Armaghani, Optimization of flyrock and rock fragmentation in the Tajareh limestone mine using metaheuristics method of firefly algorithm, Eng. Comput. (2018).
[48] J. Huang, P.G. Asteris, S. Manafi Khajeh Pasha, A.S. Mohammed, M. Hasanipanah, A new auto-tuning model for predicting the rock fragmentation: a cat swarm optimization algorithm, Eng. Comput. (2022).
[49] R. Amoako, A. Jha, S. Zhong, Rock fragmentation prediction using an artificial neural network and support vector regression hybrid approach, Mining (2022).
[50] N. Sri Chandrahas, B.S. Choudhary, M. Vishnu Teja, M.S. Venkataramayya, N.S.R. Krishna Prasad, XG boost algorithm to simultaneous prediction of rock fragmentation and induced ground vibration using unique blast data, Appl. Sci. (2022).
[51] S. Hosseini, A. Mousavi, M. Monjezi, M. Khandelwal, Mine-to-crusher policy: planning of mine blasting patterns for environmentally friendly and optimum fragmentation using Monte Carlo simulation-based multi-objective grey wolf optimization approach, Resour. Pol. 79 (2022) 103087.
[52] S. Hosseini, R. Poormirzaee, M. Hajihassani, An uncertainty hybrid model for risk assessment and prediction of blast-induced rock mass fragmentation, Int. J. Rock Mech. Min. Sci. 160 (2022) 105250.
[53] A. Zangoei, M. Monjezi, D.J. Armaghani, A. Mehrdanesh, S. Ahmadian, Prediction and optimization of flyrock and oversize boulder induced by mine blasting using artificial intelligence techniques, Environ. Earth Sci. 81 (2022) 359.
[54] A.W. Hatheway, The complete ISRM suggested methods for rock characterization, testing and monitoring; 1974-2006, Environ. Eng. Geosci. 15 (2009) 47–48.
[55] S. Nanda, B.K. Pal, Analysis of blast fragmentation using WipFrag, Int. J. Innov. Sci. Res. Technol. 5 (2020).
[56] N.H. Maerz, J.A. Franklin, L. Rothenburg, D. Linncoursen, Measurement of Rock Fragmentation by Digital Photoanalysis, 1987. ISRM-6CONGRESS-1987-127.
[57] J.A. Franklin, T. Katsabanis (Eds.), Measurement of Blast Fragmentation, first ed., Routledge, 2018.
[58] P.A. Clemenshia, C. Deepa, Enhanced factor based whale optimization algorithm with improved weight based long short-term memory for cancer subtypes diagnosis, in: 2022 International Conference on Intelligent Innovations in Engineering and Technology (ICIIET), IEEE, Coimbatore, India, 2022, pp. 260–267.
[59] J. Morgenroth, K. Kalenchuk, L. Moreau-Verlaan, M.A. Perras, U.T. Khan, A novel long-short term memory network approach for stress model updating for excavations in high stress environments, Georisk 17 (2023) 196–216.
[60] Y. Wang, G. Zheng, Y. Li, F. Zhang, Full waveform prediction of blasting vibration using deep learning, Sustainability 14 (2022) 8200.
[61] T.J. Mbah, H. Ye, J. Zhang, M. Long, Using LSTM and ARIMA to simulate and predict limestone price variations, Min. Metall. Explor. 38 (2021) 913–926.
[62] S. Mirjalili, S.M. Mirjalili, A. Lewis, Grey wolf optimizer, Adv. Eng. Software 69 (2014) 46–61.
[63] H. Faris, I. Aljarah, M.A. Al-Betar, S. Mirjalili, Grey wolf optimizer: a review of recent variants and applications, Neural Comput. Appl. 30 (2018) 413–435.
[64] J. Kennedy, R. Eberhart, Particle swarm optimization, in: Proceedings of ICNN'95 - International Conference on Neural Networks, vol. 4, IEEE, Perth, WA, Australia, 1995, pp. 1942–1948.
[65] C. Dong, G. Wang, Z. Chen, Z. Yu, A method of self-adaptive inertia weight for PSO, in: 2008 International Conference on Computer Science and Software Engineering, IEEE, Wuhan, China, 2008, pp. 1195–1198.
[66] B. Vasumathi, S. Moorthi, Implementation of hybrid ANN–PSO algorithm on FPGA for harmonic estimation, Eng. Appl. Artif. Intell. 25 (2012) 476–483.
[67] J.C. Bansal, P.K. Singh, M. Saraswat, A. Verma, S.S. Jadon, A. Abraham, Inertia weight strategies in particle swarm optimization, in: 2011 Third World Congress on Nature and Biologically Inspired Computing, IEEE, Salamanca, Spain, 2011, pp. 633–640.
[68] R.R. Ema, A. Khatun, MdA. Hossain, M.R. Akhond, N. Hossain, MdY. Arafat, Protein secondary structure prediction using hybrid recurrent neural networks, J. Comput. Sci. 18 (2022) 599–611.
[69] Z. Ding, Y. Yu, Y. Xia, Nonlinear hysteretic parameter identification using an attention-based long short-term memory network and principal component analysis, Nonlinear Dynam. 111 (2023) 4559–4576.
[70] M. Monjezi, M. Rezaei, A. Yazdian Varjani, Prediction of rock fragmentation due to blasting in Gol-E-Gohar iron mine using fuzzy logic, Int. J. Rock Mech. Min. Sci. 46 (2009) 1273–1280.

[71] S. Kumar, D. Datta, S.K. Singh, Black hole algorithm and its applications, in: A.T. Azar, S. Vaidyanathan (Eds.), Computational Intelligence Applications in Modeling and Control, vol. 575, Springer International Publishing, Cham, 2015, pp. 147–170.
[72] M.S. Kiran, TSA: tree-seed algorithm for continuous optimization, Expert Syst. Appl. 42 (2015) 6686–6698.
[73] Z. Ding, J. Li, H. Hao, Structural damage identification by sparse deep belief network using uncertain and limited data, Struct. Control Health Monit. 27 (2020).
[74] C. Kapucu, M. Cubukcu, A supervised ensemble learning method for fault diagnosis in photovoltaic strings, Energy 227 (2021) 120463.
[75] N. Kumar Bhagat, A.K. Mishra, R.K. Singh, C. Sawmliana, P.K. Singh, Application of logistic regression, CART and random forest techniques in prediction of blast-induced slope failure during reconstruction of railway rock-cut slopes, Eng. Fail. Anal. 137 (2022) 106230.
[76] X. Kong, X. Ling, L. Tang, W. Tang, Y. Zhang, Random forest-based predictors for driving forces of earth pressure balance (EPB) shield tunnel boring machine (TBM), Tunn. Undergr. Space Technol. 122 (2022) 104373.
[77] M.S. Barkhordari, D.J. Armaghani, P. Fakharian, Ensemble machine learning models for prediction of flyrock due to quarry blasting, Int. J. Environ. Sci. Technol. 19 (2022) 8661–8676.
[78] J. Zhou, P.G. Asteris, D.J. Armaghani, B.T. Pham, Prediction of ground vibration induced by blasting operations through the use of the Bayesian Network and random forest models, Soil Dynam. Earthq. Eng. 139 (2020) 106390.
[79] H. Han, D. Jahed Armaghani, R. Tarinejad, J. Zhou, M.M. Tahir, Random forest and bayesian network techniques for probabilistic prediction of flyrock induced by blasting in quarry sites, Nat. Resour. Res. 29 (2020) 655–667.
[80] Y. Dai, M. Khandelwal, Y. Qiu, J. Zhou, M. Monjezi, P. Yang, A hybrid metaheuristic approach using random forest and particle swarm optimization to study and evaluate backbreak in open-pit blasting, Neural Comput. Appl. 34 (2022) 6273–6288.
[81] B. He, D.J. Armaghani, S.H. Lai, Assessment of tunnel blasting-induced overbreak: a novel metaheuristic-based random forest approach, Tunn. Undergr. Space Technol. 133 (2023) 104979.
[82] A. Roy, R. Manna, S. Chakraborty, Support vector regression based metamodeling for structural reliability analysis, Probabilist. Eng. Mech. 55 (2019) 78–89.
[83] D. Longjun, L. Xibing, X. Ming, L. Qiyue, Comparisons of random forest and support vector machine for predicting blasting vibration characteristic parameters, Procedia Eng. 26 (2011) 1772–1781.
[84] Y. Fissha, H. Ikeda, H. Toriya, T. Adachi, Y. Kawamura, Application of bayesian neural network (BNN) for the prediction of blast-induced ground vibration, Appl. Sci. 13 (2023) 3128.
[85] E. Li, P. Segarra, J.A. Sanchidrián, S. Gómez, A. Fernández, R. Navarro, et al., Application of percentile color intensities of borehole images for automatic fluorite grade assessment, Ore Geol. Rev. 163 (2023) 105790.
[86] E. Li, J. Zhou, X. Shi, D. Jahed Armaghani, Z. Yu, X. Chen, et al., Developing a hybrid model of salp swarm algorithm-based support vector machine to predict the strength of fiber-reinforced cemented paste backfill, Eng. Comput. 37 (2021) 3519–3540.
[87] W. Zhang, H. Li, Y. Li, H. Liu, Y. Chen, X. Ding, Application of deep learning algorithms in geotechnical engineering: a short critical review, Artif. Intell. Rev. 54 (2021) 5633–5673.
[88] Y. Wang, L. Wang, S. Liu, P. Liu, Z. Zhu, W. Zhang, A comparative study of regional landslide susceptibility mapping with multiple machine learning models, Geol. J. (2023) 4902.